Cell, Vol. 97, 257–269, April 16, 1999, Copyright ©1999 by Cell Press

# The 2.8 Å Crystal Structure of Visual Arrestin: A Model for Arrestin's Regulation

**Joel A. Hirsch,[†‖] Carsten Schubert,[†‖] Vsevolod V. Gurevich,[‡] and Paul B. Sigler*[†§]**
*Howard Hughes Medical Institute
[†]Department of Molecular Biophysics and Biochemistry
Yale University
New Haven, Connecticut 06511
[‡]Ralph and Muriel Roberts Laboratory for Vision Science
Sun Health Research Institute
Sun City, Arizona 85372

## Summary

**G protein–coupled signaling is utilized by a wide variety of eukaryotes for communicating information from the extracellular environment. Signal termination is achieved by the action of the arrestins, which bind to activated, phosphorylated G protein–coupled receptors. We describe here crystallographic studies of visual arrestin in its basal conformation. The salient features of the structure are a bipartite molecule with an unusual polar core. This core is stabilized in part by an extended carboxy-terminal tail that locks the molecule into an inactive state. In addition, arrestin is found to be a dimer of two asymmetric molecules, suggesting an intrinsic conformational plasticity. In conjunction with biochemical and mutagenesis data, we propose a molecular mechanism by which arrestin is activated for receptor binding.**

## Introduction

G protein–coupled receptor (GPCR) signaling is a pathway utilized by a wide variety of eukaryotic organisms to communicate signals from the environment. These signals range from photons to small molecule neurotransmitters and odorants to polypeptide hormones. The signals themselves activate membrane-embedded receptors, which have characteristic seven-transmembrane regions, by inducing a conformational shift whereby the activated receptor catalyzes the nucleotide exchange of heterotrimeric G proteins. The G protein subunits then propagate the signal to a variety of effector molecules whose activities lead to physiological responses by the cell.

Cellular downregulation of this signaling pathway is fine-tuned by a large cast of macromolecules (reviewed in Krupnick and Benovic, 1998; Lefkowitz, 1998). The enzymatic activity of the receptor on its substrate, G protein, is slowed by phosphorylation of the receptor through the action of specific receptor kinases. Subsequently, a family of intracellular inhibitory proteins dubbed arrestins terminate receptor activity. They bind the cytoplasmic surface of the receptor, thereby occluding interaction with the G proteins, a process referred to as desensitization. Some arrestins also serve as adaptor molecules to the cellular protein trafficking machinery, facilitating the receptor's sequestration by endocytosis. This regulatory process is integrated with receptor function such that the kinase will only phosphorylate activated receptors and the arrestins will only associate with a receptor if it has been previously phosphorylated.

The visual system is one of the best-studied GPCR signaling pathways and has served as a paradigm for its mode of action. In particular, the retinal rod cell and its receptor, rhodopsin, provide a model for the pathway due to its low noise, exquisite sensitivity, and enormous dynamic range. Moreover, vision demands far greater time resolution than other GPCR-mediated processes; therefore, rhodopsin kinase and visual arrestin must quench the activated receptor very quickly. Thus, visual arrestin serves as a rapid, sensitive, and explicit "off switch" with selectivity for the cognate receptor that is both activated and phosphorylated. This strong selectivity is more pronounced in visual arrestin than other members of the family (Gurevich et al., 1995).

We describe here the 2.8 Å crystal structure of recombinant bovine visual rod arrestin, which together with biophysical, biochemical, and mutation studies, provides a structural framework for the molecular mechanism of arrestin and especially its proposed novel form of regulation. For reasons made clear below and in a companion paper (Vishnivetskiy et al., 1999), we believe the conformation of free arrestin seen in this crystal structure is designed to resist a stable interaction with the receptor. It is the allosteric effect of the phosphorylated C-terminal segment of the receptor that alters arrestin's conformation, thereby promoting its binding to the activated receptor.

## Results and Discussion

### Structure Determination

Recombinant visual arrestin was expressed and purified as described in Experimental Procedures. Two crystal forms were obtained at 4°C that diffracted to moderate resolution. One form was solved and refined to 2.8 Å resolution (C form); the other (P form) was solved by molecular replacement using the structure of the C form as the search model and refined to 3.4 Å. As detailed below, each crystal form contains four molecules of arrestin in the asymmetric unit. Two of these have one conformation (α) and two have a somewhat different conformation (β). They are arranged such that one pair (αβ) is related by a local two-fold rotation axis to a second pair (α′β′). The lattice is sparsely packed in both crystal forms, leading to weak diffraction and making synchrotron radiation mandatory. Electron density maps (Figure 1) were phased with multiple wavelength anomalous diffraction from 23 selenomethionine-substituted positions as well as both isomorphous and anomalous scattering differences from heavy atom replacements.

[§]To whom correspondence should be addressed (e-mail: sigler@csb.yale.edu).
[‖]These authors contributed equally to this work.

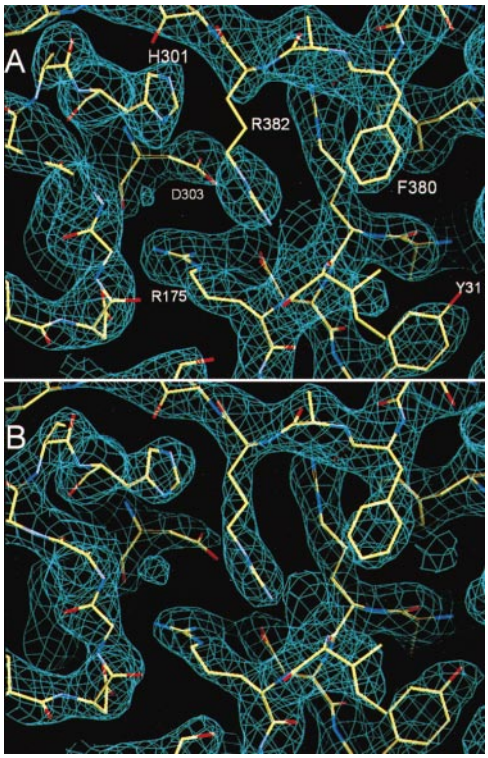


Figure 1. Electron Density

(A) Diagram of the solvent-flattened experimental electron density, contoured at 1.5 σ, showing parts of the polar core. The density for Phe-380 is clearly discernible in the experimental map, supporting our assignment of the C tail.

(B) Experimental phase combined 2Fo-Fc map, contoured at 1.8 σ, from the same region. Figures generated with O (Jones et al., 1991).

The current model includes residues 8–362 and 372–394. Although density is present in experimental maps, residues 363–371 have been modeled as polyalanine, owing to their poorly defined nature, probable partial occupancy, and high mobility. Similarly, residues 395–402 have been modeled as polyalanine for molecules α and α′ only, and their placement is provisional. No density is discernible for the amino-terminal six residues.

A crystal structure of visual arrestin from bovine retinae in the P crystal form was reported at 3.3 Å resolution (Granzin et al., 1998). The structure described here differs significantly in biologically relevant ways from the previous report.

## Molecular Architecture

Each molecule is composed of two domains where each domain is constructed from a seven-stranded β sandwich (Figures 2 and 3A). The sandwich comprises a four-stranded β sheet packed against a three-stranded β sheet. Each domain contains an additional lateral strand. The two domains, named N domain (residue 8–180) and C domain (residue 188–362), are related by an intramolecular pseudo two-fold rotation axis. The N domain is adorned with a single α helix, while the C domain contains two short $3_{10}$ helices in a long loop that provides some of the interface between the two domains. The very carboxyl terminus of the protein or "C tail" (residues 372–404) is connected by a flexible linker (residues 362–371) to the C domain. The C tail contains a short stretch that forms a parallel β sheet interaction with the lateral strand of the N domain. In addition, the C tail makes other interactions with various parts of both the N and C domains. The dimensions of the molecule are approximately 95 × 45 × 60 Å.

Arrestin appears to have a novel structure. A search using the FSSP algorithm (Holm and Sander, 1998) for similar structures yielded only previously solved β sandwich modules as observed in the N and C domains. No structures in the PDB remotely resemble the topology and domain orientation of full-length arrestin. The topology diagram (Figure 3A), as well as the Cα trace of the refined model, indicates strong structural similarity between the N and C domains. This structural similarity is only marginally reflected in a 19.3% sequence identity (ALIGN) (Myers and Miller, 1988). In contrast, a rotation of 158° superimposes 97 of the 175 Cα atoms with a root-mean-square deviation (rmsd) of 1.8 Å and a P value of $10^{-22}$ (Gerstein and Levitt, 1998). This P value underscores the superimposition's statistical significance.

The structural homology between domains is far stronger than any homology with previously described structures. The relatedness of the two individual domains, their topological independence, and particularly their arrangement relative to each other bear directly on their potential for conformational adjustments by en bloc domain rearrangements. Such shifts would be consistent with arrestin's activation, as described below.

Alignment of nine arrestin sequences based on this structure indicates that all members of this family will maintain a very similar fold (Figure 4). The most distant sequence, that of *C. elegans*, contains only two significant inserts located in the loops between secondary structural elements. The alignment suggests that critical segments and residues implicated in function are highly conserved. Clearly, there are two major families of arrestin, one used in the visual systems (rod and cone) and the other used in the balance of tissues. The two families are distinguished by an insertion between the C domain and the C tail (see below). This segment has been implicated in the interaction with clathrin endocytic desensitization (Krupnick et al., 1997).

## Oligomerization

Both crystal forms have an asymmetric unit comprising an arrestin tetramer. As noted above, there are two α molecules and two β molecules, where α and β differ only in their conformation. The protomers (an αβ dimer) are related by a single noncrystallographic two-fold axis. Hence, the arrangement is a symmetrical dimer of αβ heterodimers. The noncrystallographic two-fold symmetry facilitated the structure analysis. However, the transformation relating the α and β molecules within the protomeric dimer was not used; rather, both α and β were built independently.

The quaternary structure observed in both crystal forms and in the previously reported structure is the same. This observation suggests that the oligomerization in the crystal is inherent to the chemistry of arrestin rather than an artefact of the crystal packing and led us

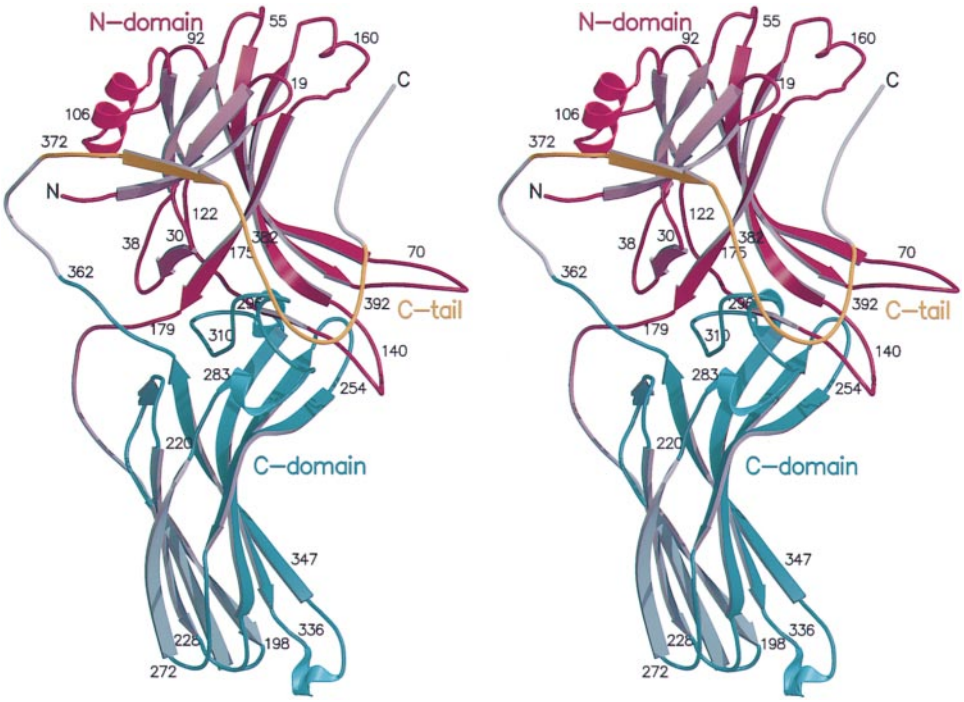


Figure 2. Structure of Arrestin

Stereo diagram of a ribbon drawing of the α conformer. The N and C domains are coded in pink and cyan, respectively; disordered regions are shown in gray. Figure made with MOLSCRIPT/RASTER3D (Kraulis, 1991; Merritt and Bacon, 1997).

to investigate whether the same quaternary structure was detectable in solution and is possibly biologically relevant. A comprehensive analytical ultracentrifugation study was undertaken (C. S. et al., submitted). The solution experiments indicate that, at high concentration (200 μM), arrestin is best modeled as a tetramer. However, at lower concentrations, arrestin participates in a monomer/dimer equilibrium with a $K_D = 34 (\pm 4)$ μM. The most likely pairing of subunits in the dimer is shown in a partial view in Figure 5C (C. S. et al., submitted). The dimer interface between α and β involves two loci of interactions (Figures 5C and 5E). Importantly, dimerization of α and β buries 2100 Å$^2$ of solvent-exposed surface area, a value that is well in the range for functional dimers in solution (Jones and Thornton, 1995).

Does the oligomerization observed in the crystal structures and centrifugation data have any physiological relevance, and might it occur in vivo? Arrestin is the second most abundant soluble protein in the rod outer segment (ROS). Estimates of its concentration range from 50 to 167 μM (Hamm and Bownds, 1986; Kawamura, 1995). Hence, a significant fraction of the arrestin population in ROS will be dimeric. However, we know that arrestin is active as a monomer, since concentration conditions where rhodopsin binding experiments are performed are in the monomeric regime. Assuming that the dimer is characteristic of the inactive state, its dissociation might serve as an autoregulatory mechanism whereby the steady-state concentration of monomeric arrestin is held at the desired level. This mechanism provides a large reserve of rapidly available arrestin when conditions require prompt and substantial desensitization while preventing high concentrations of monomeric arrestin from prematurely squelching a signal.

**Role of Arrestin Plasticity**

Molecules α and β of the heterodimer represent conformationally different molecules. The rmsd of α and β upon superposition is 3.0 Å for Cα atoms only. The large difference is attributable to three discrete regions, residues 68–79 (i), 155–165 (ii), and 337–347 (iii) (Figure 5); if one excludes those regions and some short secondary elements and linkers, the structure is the same (rmsd = 0.7 Å for 338 Cα atoms). Region ii highlights the remarkable plasticity of the protein. In α, region ii takes a helical conformation, whereas in β, it forms a strand-turn-strand, forming an antiparallel β sheet interaction with a neighboring crystallographic symmetry mate. The sequence falls into a hitherto rare but now emerging class of polypeptides, called "chameleons" by Kim and coworkers, whose conformation is determined by global environment rather than sequence (Minor and Kim, 1996). Recently, another natural chameleon structure was observed in the MCM protein dimer (Tan and Richmond, 1998).

A conformational heterodimer of proteins with identical sequences in the same crystal is not unprecedented. Antithrombin, a member of the serpin class of protease inhibitors, exhibits a similar behavior wherein one of the molecules of the dimer is found in the active state and the other in the latent state (Carrell et al., 1994; Schreuder et al., 1994). In antithrombin, the two conformations represent bona fide biologically relevant conformers. Likewise, arrestin's observed plasticity may permit alternate local surfaces that the molecule will present upon association with other macromolecular partners such as a receptor. Indeed, regions i and ii (especially region i) contain both some degree of sequence conservation and solvent accessibility (Figure

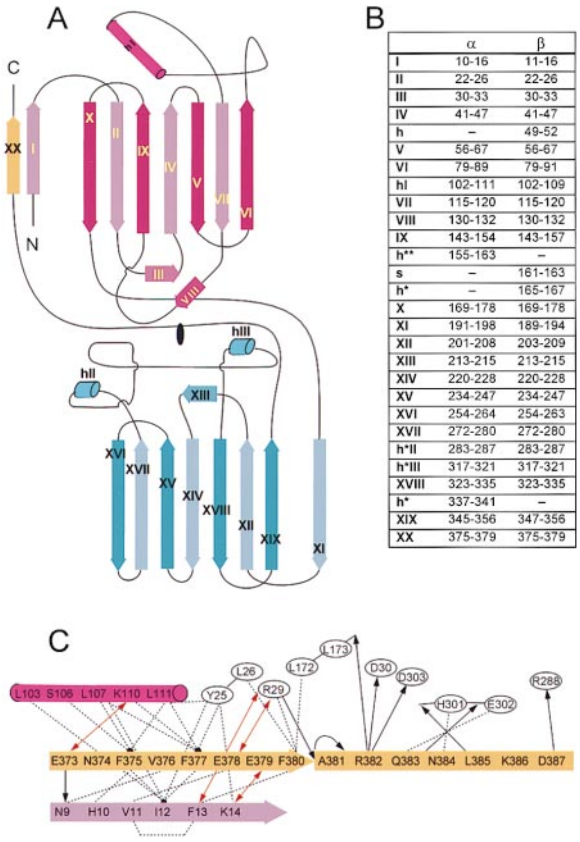


B

| | α | β |
|---|---|---|
| I | 10-16 | 11-16 |
| II | 22-26 | 22-26 |
| III | 30-33 | 30-33 |
| IV | 41-47 | 41-47 |
| h | – | 49-52 |
| V | 56-67 | 56-67 |
| VI | 79-89 | 79-91 |
| hI | 102-111 | 102-109 |
| VII | 115-120 | 115-120 |
| VIII | 130-132 | 130-132 |
| IX | 143-154 | 143-157 |
| h** | 155-163 | – |
| s | – | 161-163 |
| h* | – | 165-167 |
| X | 169-178 | 169-178 |
| XI | 191-198 | 189-194 |
| XII | 201-208 | 203-209 |
| XIII | 213-215 | 213-215 |
| XIV | 220-228 | 220-228 |
| XV | 234-247 | 234-247 |
| XVI | 254-264 | 254-263 |
| XVII | 272-280 | 272-280 |
| h*II | 283-287 | 283-287 |
| h*III | 317-321 | 317-321 |
| XVIII | 323-335 | 323-335 |
| h* | 337-341 | – |
| XIX | 345-356 | 347-356 |
| XX | 375-379 | 375-379 |




Figure 3. Topology of Arrestin and Interactions of the C Tail

(A) Folding pattern of arrestin showing the arrangement of secondary structure elements. The color coding is the same as in Figure 2; the C tail is displayed in yellow. Strands lying in the same sheet of a β sandwich are distinguished by light and dark hues. The internal pseudo two-fold rotation axis is indicated by the black oval.

(B) Difference in secondary structure assignments between molecules α and β. Strands in common are indicated by roman numerals; α helix by h; $3_{10}$ helix by h*; helical conformation by h**; strand by s. Secondary structure assignment is based on DSSP (Kabsch and Sander, 1983).

(C) Schematic overview of the C tail (yellow) contacts separated into electrostatic interactions (red arrows), hydrogen bond interactions (black arrows), and van der Waals contacts (dotted lines). The hydrogen bonds of the parallel β sheet interactions between strand I and strand XX have been omitted for clarity.

4), suggestive of their functional importance for conserved intermolecular interactions and not for folding or architectural considerations within the molecule itself.

**The Polar Core of the Basal State**

Figure 6A shows the most distinctive feature of arrestin's conformation, namely a polar core embedded between the N and C domains in the fulcrum of the molecule. This core structure comprises charged residues from the very N terminus (Asp-30), the body of the N domain (Arg-175 and Lys-176), the interfacial loop of the C domain (Asp-296 and Asp-303), and the C tail (Arg-382). These residues share a very high degree of sequence conservation, implying that the structure of this core region is conserved among all arrestins and is doubtless critical for function. Aside from exhibiting an elaborate network of hydrophobic and hydrogen bond interactions, the striking feature of this core is the degree to which these charged side chains are buried. Lys-176, Arg-382, Arg-175, and Asp-296 have a total fractional accessibility index of less than 10% (Lee and Richards, 1971), whereas Asp-30 and Asp-303 are partially solvent accessible, with values of 25% and 35%, respectively. Arrestin achieves sufficient charge neutrality to maintain its structure by forming charge–charge interactions between Arg-382–Asp-30–Asp-303 and Arg-175–Asp-296. Both computational and experimental work recently have shown that the burial of ion pairs is, in general, energetically unfavorable (Hendsch and Tidor, 1994; Waldburger et al., 1995; Wimley et al., 1996; Sindelar et al., 1998). A network of buried ion pairs such as that observed here must impart an important function to the molecule and/or specify a particular molecular architecture in order to justify its energetic cost.

The polar core also provides a mechanism for facile reorganization of the structure. Unlike the usual hydrophobic core of globular proteins whose structure accommodates a wide range of changes in side chain packing by small local adjustments in the fold (Lim and Sauer, 1989; Matthews, 1995), changes in the delicate balance of electrostatic charge in the polar core's solvent-shielded environment are likely to lead to its substantial disruption.

The functional significance of this unique polar core may lie in the role that receptor phosphorylation plays in regulating the affinity of arrestin for the receptor. Phosphorylation of the cytoplasmic C-terminal segment of the activated receptor is the molecular switch that triggers arrestin's ability to avidly bind and inactivate the receptor. It is clear that a specific arrestin-binding surface is not being created by phosphorylation of the C-terminal segment, since phosphorylation at any one or more of seven serine/threonine residues can activate the arrestin response (Aton et al., 1984; McDowell et al., 1993; Ohguro et al., 1994a, 1995). Rather, the biochemical and mutagenesis data suggest that a phosphorylated C-terminal segment represents a reagent closely tethered to the receptor's surface that can activate arrestin, which normally exists in an inactive conformation (basal state). We believe that the intrusion of a phosphate moiety in or near the polar core would electrostatically destabilize this electroneutral network of polar interactions and lead to significant rearrangement of arrestin's conformation from the basal state visualized in the crystal structure to an active state that enables receptor binding.

The proposed disruption of the polar core can be partially emulated by mutational changes. Mutations that alter Arg-175, especially R175E (Gurevich and Benovic, 1997) (Figure 6B), abolish arrestin's ability to distinguish between Rho*-P (light-activated, phosphorylated rhodopsin) and Rho* (light-activated, nonphosphorylated rhodopsin), suggesting that this critical arginine residue is at the center of the phosphorylation-sensitive trigger. The structure shows that Arg-175 interacts with its negatively charged partners, constraining the molecule to its basal state. An electrostatic molecular surface representation (Figure 7B) shows that Arg-175 is located on the bottom of a deep positively charged groove. This groove appears to be the most likely access route to

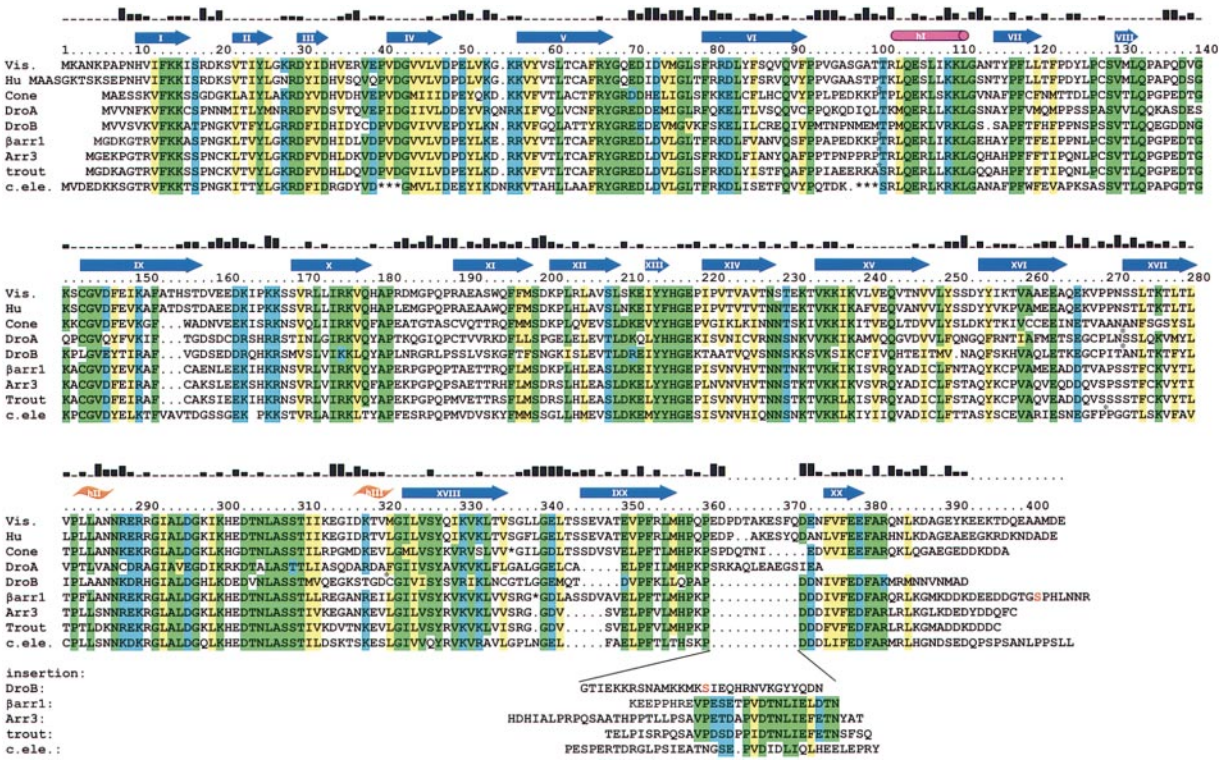








Figure 4. Sequence Alignment and Structural Features of Arrestin

Sequence alignment between bovine visual arrestin (SWISSPROT accession number P08168), human rod arrestin (P10523), *X. laevis* cone arrestin (P51483), *D. melanogaster* arrestins A and B (P15372, P19107), rat β-arrestin1 (P29066), bovine arrestin3 (P32120), trout arrestin (P51466), and *C. elegans* arrestin (P51485). Green highlighting indicates highly conserved residues (8 of 9 identical), blue indicates conservative substitutions, and conserved hydrophobic residues are highlighted in yellow. Surface accessibility is indicated by the height of the histograms above the corresponding residue. Residues that could not be modeled with confidence are indicated as dots. Inserts (asterisks) were omitted from the alignment for clarity, except for the insertion between residues 360 and 370, which contains the conserved clathrin-binding site in the β-arrestin family. Phosphorylation sites are in red.

the polar core for the negatively charged C-terminal segment of Rho*-P, since the opposite side of the molecule as depicted in Figure 7B is blocked by the negative surface potential induced by Asp-296, Asp-30, and Asp-303. We posit that upon arrestin's interaction with rhodopsin's phosphorylated C-terminal segment, the polar core interactions are disrupted and considerable rearrangement of arrestin occurs, indicated by the high Arrhenius activation energy of 140 kJ $mol^{-1}$ of binding to Rho*-P (Schleicher et al., 1989; Pulvermüller et al., 1997).

Following a simplistic coulomb repulsion approach, one would expect that reversing the charge of any of the aspartate residues in the polar core would yield the same binding response as R175E, thus providing a simple explanation for the mechanism of action. But the mutation that has the most significant effect is D296R (Vishnivetskiy et al., 1999) (Figure 6B). Asp-296 is located in a "lariat" loop (residues 283–304, blue chain in Figure 6A). The lariat is part of the interface between the N and C domains. D296R is the only aspartate mutation that binds nonphosphorylated Rho* in significantly enhanced levels in a manner similar to R175E. Moreover, R175E/D296R (Vishnivetskiy et al., 1999) is the only single charge swap that restores wild-type activity. Together with the structural information, these data demonstrate that Asp-296 and Arg-175 form an electrostatically and structurally important ion pair that is the most critical one in maintaining arrestin's basal state. Disruption of this interaction leads to a constitutive enhancement of arrestin's affinity for the receptor, drastically decreasing its regulatory discrimination.

## C Tail: Structure and Function

The C tail was shown to be a crucial regulator for arrestin's discrimination against Rho* (Palczewski et al., 1991a). Its absence in the $p^{44}$ splice variant (Palczewski et al., 1994) (residues 1–370) or its proteolytic removal (Palczewski et al., 1991b) parallels to some degree the relaxation of specificity caused by charge reversal mutations (e.g., R175E) in the polar core. Thus, unlike full-length arrestin, $p^{44}$ binds to Rho*, as well as to Rho-P (dark adapted, phosphorylated rhodopsin). Moreover, the activation energy required to bind Rho*-P is reduced in half, from 140 kJ $mol^{-1}$ to 70 kJ $mol^{-1}$ (Pulvermüller et al., 1997). The structural basis for the C tail's role in restraining arrestin in the inactive state is outlined in Figures 3C and 6. The C tail participates in an extensive network of mutagenically sensitive electrostatic, van der Waals, and hydrogen-bonded interactions including those made by Arg-382 with Asp-30 and Asp-303, as noted earlier in the description of the polar core.

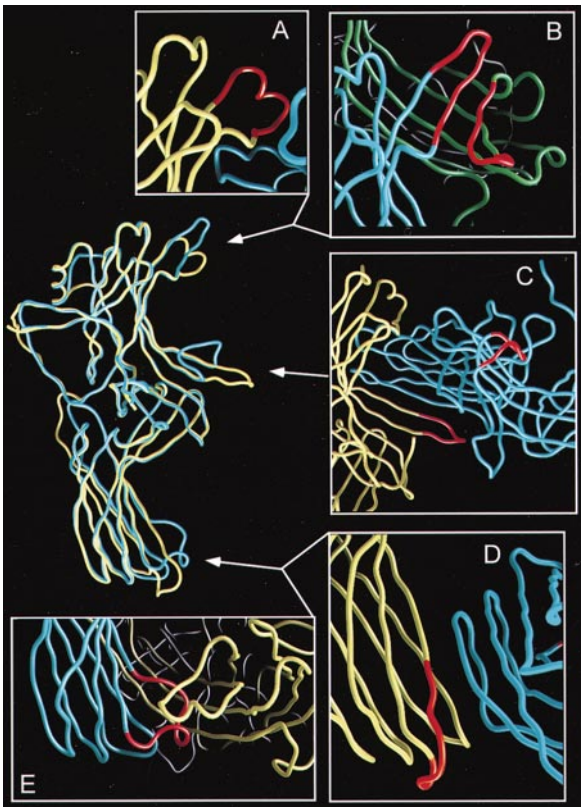


Figure 5. Plasticity of Arrestin and the αβ Dimer Interface

The central part of the figure shows a superposition of arrestin conformers, with α (yellow) and β (cyan) drawn with the same orientation as Figure 2. The red highlighted segments are those that differ in α and β due to the global environment.

(A) The helical conformation of residues 155–165 (region ii in the text).

(B) Region ii takes a strand-turn-strand conformation. Interface between β and the crystallographic symmetry mate of β′ (green).

(C) Residues 68–79 (region i in the text) are depicted. In α, they are in an extended strand conformation, making β sheet interactions, whereas in β, they collapse into a loop. A portion of the dimer interface between α and β is a parallel strand interaction, forming a continuous sheet from one molecule to the next. This area extends over ten residues and involves side chain interactions as well.

(D) Interface between α and β′ (cyan). Residues 337–347 (region iii in the text) in α are in the strand conformation, involved in sheet interactions with a molecular partner.

(E) Dimer interface between α and β; region iii in β is in an odd loop conformation. This portion of the αβ interface is noteworthy due to its unusual interclasping of rolled sheet surfaces. Figure made with GRASP (Nicholls et al., 1991).

### Model for Arrestin's Activation

Based on the structural, biochemical, and mutational information, we present a model that explains how arrestin's activity is regulated. We propose that the basal state is maintained by the critical hydrogen-bonded salt bridges of the polar core and by interactions of the regulatory C tail. Upon binding, the receptor's negatively charged phosphate ester disrupts the polar core and releases the C tail of arrestin. Together these events lead to a reorientation of the N and C domains that favors the binding of arrestin to the activated, phosphorylated receptor. The disruption of the constraints would permit a structural reorganization and thereby facilitate the formation of an arrestin–receptor complex. This model is consistent with the effect of splicing, truncation, and proteolytic modifications that, on the basis of the structure, would likely destabilize the polar core and mitigate the stabilizing influence of the C tail. Such arrestin variants retain their affinity for Rho*-P but lose their ability to discriminate against Rho* (Gurevich et al., 1994; Palczewski et al., 1994).

The model calls for the release of activated arrestin's C tail, which is compatible with the C tail's increased accessibility to lysine modification (Ohguro et al., 1994b) and accelerated proteolysis in the presence of Rho*-P and not Rho*, a result that can also be induced by the negatively charged heparin and the isolated phosphorylated C-terminal segment of rhodopsin alone (Palczewski et al., 1991b; Puig et al., 1995). For example, experiments with bovine calpain II (Azarian et al., 1995), a protease that specifically cleaves between Phe-377 and Glu-378, demonstrated that arrestin's C tail is sensitive to proteolytic cleavage only in the presence of Rho*-P.

Another functional role of the C tail's displacement upon arrestin binding to rhodopsin implies the unmasking of binding sites for the receptor (Figure 8). Consistent with this role, mutation of Leu-172 to Ala (Gurevich and Benovic, 1997) diminishes binding to Rho*-P by 50%. With the C tail bound, as seen in the crystal structure, Leu-172 is completely shielded (fractional accessibility ≈ 0%) but would become much more accessible (14%) upon release of the C tail.

Mutagenesis experiments show that in addition to the stabilization provided by Arg-382 of the C tail (Vishnivetskiy et al., 1999), other residues help maintain the basal state in a form that prevents binding to Rho*. The crystal structure indicates that mutations which change Phe-375 and Phe-377 to Ala (Gurevich, 1998) would disrupt the interactions between these hydrophobic residues of the C tail and helix I as well as strand I. These mutations result in a relaxation of specificity in the receptor binding profile that resembles that of $p^{44}$, in which the C tail is absent. Deletions of residues 11–16 of the N terminus, which interact with residues 375–377 (Figure 3C), also show a selectivity profile exhibiting markedly increased Rho* binding (Vishnivetskiy et al., 1999).

Finally, the importance of the C tail in arrestin's regulatory function is underlined by the fact that the majority of the residues in the C tail, as well as the polar core, that stabilize the basal state and allow binding only to Rho*-P are highly conserved among all arrestins (Figure 4). This conservation suggests that the structural basis for the mechanism of activation proposed for visual arrestin is shared among all members of this molecular family.

Our assignment of the C-terminal part of arrestin differs with the previous reported structure of arrestin (Granzin et al., 1998), where the C terminus could only be traced to residues 363 and 368 for molecules α/α′ or β/β′, respectively. Rather, the first nine residues of the N terminus were assigned positions where we place residues 375–384. There are multiple reasons why we believe that our assignment is correct. First, experimental maps from this region (Figure 1) show unambiguous side chain density for the aromatic residues of the C tail (Phe-375, Phe-377, Phe-380, and Tyr-391). Second, mutations that disrupt the polar core should lead to profound functional changes; however, mutations that

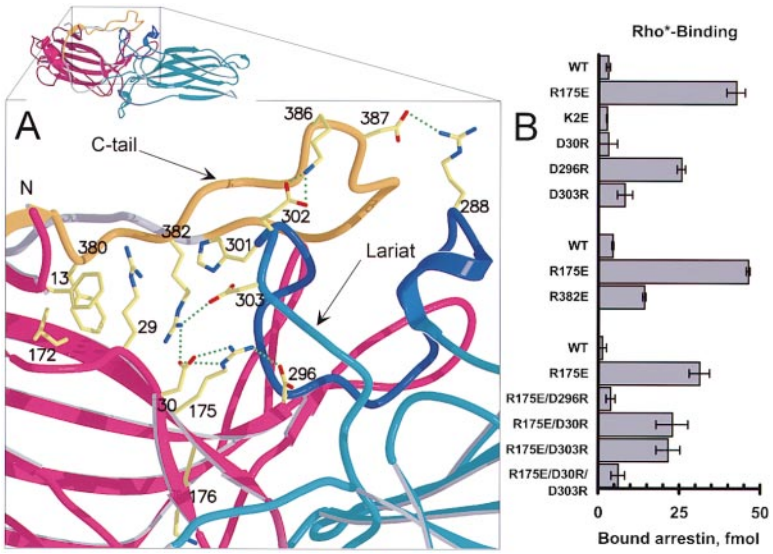


Figure 6. Close-Up View of the Polar Core and the Functional Consequences of Its Perturbation

(A) Illustration of the hydrogen-bonded interactions (green dotted lines) between residues in the polar core including contributions from the C tail and the lariat. The color coding is the same as in Figure 2 except for the depiction of the lariat loop from the C domain, which is in blue. Figure made with MOLSCRIPT/RASTER3D.

(B) Histogram depicting the effect of mutations in the polar core upon the binding to Rho* as determined in three separate experiments. All mutants bind Rho*-P and do not bind Rho, essentially as wild type (WT). WT and R175E are included as negative and positive controls for each series of experiments. For additional data and experimental detail, see Vishnivetskiy et al. (1999).

alter Lys-2 (Figure 6B), which in the previously reported structure contributes to the polar core, have no effect on the binding characteristics of arrestin (Vishnivetskiy et al., 1999). In our model, Arg-382 occupies the same position as Lys-2 does in the previously reported structure. Mutations of Arg-382, as noted earlier, show significant binding to Rho* (Vishnivetskiy et al., 1999) (Figure 6B). We therefore believe that the positional assignment of Lys-2 and the associated N terminus in the structure of Granzin et al. (1998) is in error. Third, proteolysis studies (Palczewski et al., 1991a) indicate that the very N terminus of arrestin is flexible, since trypsin is able to cleave off the first two residues including Lys-2, a result

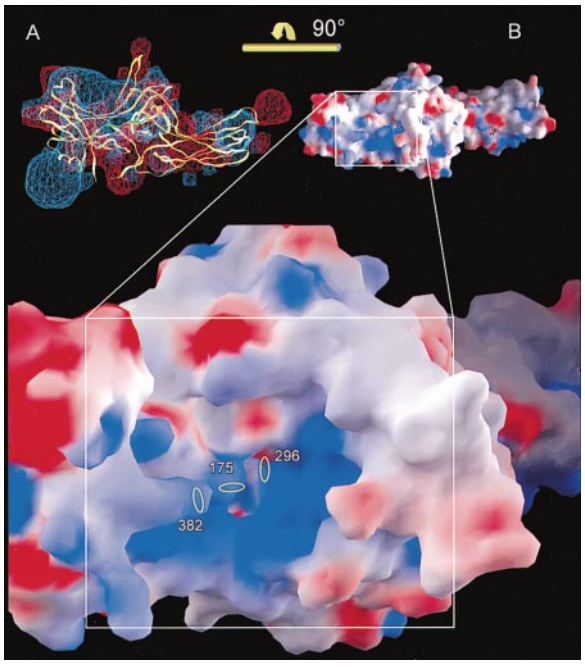


Figure 7. Electrostatic Potential Representation of Arrestin

Electrostatic potential of arrestin contoured at 1.5 kT (blue) and −1.5 kT (red) (ionic strength equivalent 0.1 M NaCl). The potential map (A) is calculated with a model excluding marginally ordered and disordered residues (i.e., 2–6, 364–373, and 395–404). The ordered part of the C tail is drawn in green. The N domain is the left half, and the C domain is the right half of the molecule. (B) shows the positive patch of charge potential on the N domain projected onto a molecular surface representation. The location of the head groups of three essential polar core residues is outlined in the inset. Note that these side chains are actually below the surface facing away from the viewer. Figure generated with GRASP.

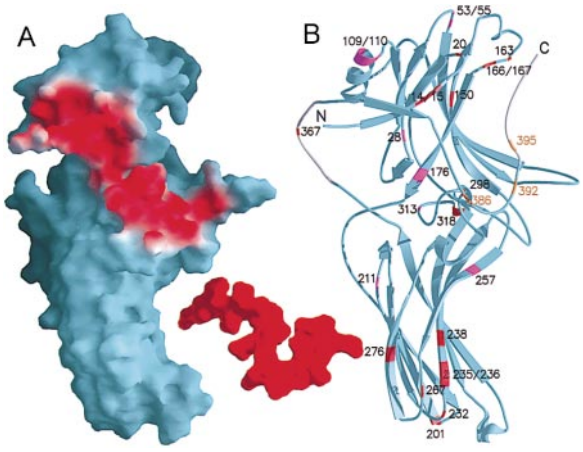


Figure 8. Footprint of the C Tail and Lysine Accessibilities

The footprint of the C tail on the molecular surface of arrestin is illustrated in (A). Red colors indicate a 4 Å distance or less between the C tail and the remainder of the molecule. The C tail's molecular surface (red) has been detached and shifted away from the body of the molecule. (B) shows the difference in the accessibility of lysines toward acetylation upon binding of arrestin to Rho*-P compared to background binding to Rho-P (based on Figure 6, 2 mM panel, from Ohguro et al., 1994b). This either maps possible contact points with the receptor or indicates locations of structural rearrangements upon binding of arrestin to activated rhodopsin. Red indicates lysine residues that become more protected by Rho*-P; orange, become more exposed by Rho*-P; purple, no detectable change. The molecular orientation is the same as Figure 2. Figures made with GRASP and MOLSCRIPT/RASTER3D, respectively.

Table 1. Crystallographic Statistics

Data Collection Statistics (Class A)

| Data set | $\lambda_3$ "Low Remote"[c] | $\lambda_1$ "Peak" | $\lambda_2$ "Inflection" | $\lambda_4$ "High Remote" | Se-Met | $K_2Pt(CN)_4$ | Ethyl Mercury Phosphate | Native |
|---|---|---|---|---|---|---|---|---|
| Beamline[a] | ID19 | ID19 | ID19 | ID19 | A1 | X25 | X25 | A1 |
| Wavelength (Å) | 1.0332 | 0.97921 | 0.973934 | 0.9393 | 0.908 | 1.1 | 1.006 | 0.908 |
| Resolution (Å) | 24–3.15 | 24–3.2 | 24–3.3 | 24–3.6 | 39–3.45 | 20–3.1 | 38–3.4 | 44–3.5 |
| Observed/unique | 342,375/51,936 | 338,693/48,052 | 334,957/47,325 | 247,877/35,650 | 89,434/23,498 | 209,271/54,659 | 101,889/32,492 | 147,352/37,512 |
| $R_{sym}$ (%)[b] | 7.1 (31.7) | 9.6 (33.6) | 8.7 (30) | 8.9 (29.1) | 6.2 (16.2) | 5.9 (30.1) | 9.0 (27.5) | 9.6 (22.9) |
| $R_{meas}$ (%)[b] | 7.7 (36.3) | 10.3 (36.5) | 9.4 (32.6) | 9.6 (31.5) | 7.4 (21.1) | 6.8 (36) | 10.6 (33.5) | 11 (27.4) |
| $R_{anom}$ (%)[h] | 4.0 | 7.0 | 6.9 | 5.9 | | | | |
| Redundancy[b] | 6.6 (4.3) | 7 (6.7) | 7.1 (6.7) | 7 (6.9) | 3.1 (1.6) | 3.8 (3.2) | 3.1 (2.8) | 3.9 (2.9) |
| Completeness (%)[b] | 98 (86.2) | 99.7 (99.2) | 99.7 (99.2) | 99.7 (99.9) | 69.3 (35.9) | 98.3 (93.7) | 76.1 (67.5) | 94.7 (91.8) |
| $I/\sigma$[b,e] | 7.4 (2.2) | 6.4 (2.4) | 6.2 (2.4) | 6.6 (2.1) | 8.2 (3.1) | 19.3 (4.2) | 5.8 (2.5) | 12.4 (4.8) |
| Combined MAD/MIRAS Refinement | | | | | | | | |
| $R_{iso}$ | | 10.8 | 7.3 | 7.4 | 11.0 | 18.5 | 27.5 | 12.6 |
| f′/f″ | −2.51/0.55 | 0.0/8.44 | −2.52/9.02 | −6.18/3.59 | −0.5/3.6[g] | −9.2/4.1 | −13.3/8.4[g] | |
| Phasing $power_{cen/iso}$ | | 0.23 | 0.02 | 0.5 | 0.44 | 0.77 | 1.38 | 0.99 |
| Phasing $power_{acen/iso}$ | | 0.35 | 0.005 | 0.64 | 0.64 | 0.96 | 1.68 | 1.28 |
| Phasing $power_{acen/ano}$ | 0.48 | 2.8 | 3.11 | 1.61 | 1.86 | NA | 1.59 | NA |
| Figures of merit | 0.641 (centrics) | 0.727 (acentrics) | | | | | | |

Data Collection Statistics (Class B)

| Data set | "Pseudo"-Native[c] | Derivative 1 | Derivative 2 | Derivative 3 | Derivative 4 | Native 2 | Native 3 | "Pseudo"-Native 4 | "P Form" |
|---|---|---|---|---|---|---|---|---|---|
| Compound | 10 mM $PbAc_2$ | 0.9 mM $K_2IrCl_6$ | 10 mM $(NH_4)_2WS_4$ | 230 μM $CH_3HgCl$ | 4 mM $(CH_3)_3PbAc$ | 1 mM $MgAc_2$ | 1 mM $MgAc_2$ | 10 mM $PbAc_2$ | |
| Beamline[a] | F1 | X25 | F1 | X25 | X25 | ID19 | ID19 | ID19 | F1 |
| Wavelength (Å) | 0.9188 | 1.1058 | 0.9188 | 1.01 | 0.972 | 1.00523 | 1.10588 | 1.00523 | 0.9188 |
| Resolution (Å) | 43–2.8 | 30–3.15 | 44–3.5 | 30–3.5 | 38–3.6 | 43–2.9 | 24–3.25 | 43–3.17 | 45.2–3.2 |
| Observed/unique | 242,164/64,227 | 457,872/53,536 | 256,418/37,764 | 177,116/33,788 | 243,432/42,787 | 222,951/63,595 | 202,718/48,800 | 209,840/52,529 | 129,656/39,693 |
| $R_{sym}$ (%)[b] | 5.1 (35.3) | 7.3 (34.0) | 9.8 (29.7) | 7.6 (26.8) | 7.7 (34.0) | 7.3 (31.9) | 6.3 (30.4) | 7.4 (33.7) | 6.2 (29.6) |
| $R_{meas}$ (%)[b] | 5.8 (48.4) | 7.7 (36.7) | 11.2 (36.3) | 8.5 (29.7) | 8.4 (37.9) | 8.6 (40.7) | 7.2 (35.1) | 8.5 (38.7) | 7.2 (38.1) |
| Redundancy[b] | 3.8 (1.5) | 8.6 (7.2) | 4.1 (2.6) | 5.2 (5.1) | 5.7 (4.7) | 3.5 (2.0) | 4.2 (3.9) | 4.0 (4.1) | 3.3 (1.9) |
| Completeness (%)[b] | 84.1 (38) | 99.2 (88.4) | 96.9 (89.2) | 85.2 (85.7) | 99.4 (97.6) | 90 (42.9) | 99.4 (99) | 99.8 (99.9) | 82.4 (61.2) |
| $I/\sigma$[b,e] | 11.1 (2.3) | 7.7 (2.1) | 6.0 (2.6) | 19.2 (4.3) | 7.9 (1.6) | 6.2 (2.1) | 9.5 (2.2) | 7.6 (2.2) | 8.4 (2.3) |
| MIRAS Refinement (44–2.8 Å) | | | | | | | | | |
| $R_{iso}$ | | 15.8 | 23.5 | 27.5 | 17.9 | 8.5 | 12.0 | 10.1 | |
| f′/f″ | | −14.89/12.14[g] | −3.11/8.52[g] | −12.1/4.81[g] | −8.99/7.88[g] | | | | |
| Phasing $power_{cen/iso}$ | | 0.86 | 1.77 | 1.38 | 1.22 | NA | NA | NA | |
| Phasing $power_{acen/iso}$ | | 1.05 | 2.3 | 1.78 | 1.58 | NA | NA | NA | |
| Phasing $power_{acen/ano}$ | | 1.64 | 1.83 | 1.7 | 1.11 | | | | |
| Figures of merit | 0.422 (centrics) | 0.469 (acentrics) | | | | | | | |

*continued*

Table 1. Continued

| Refinement Statistics[d] | Class A | Class B | P Form |
|---|---|---|---|
| No. of reflections (working, test)[f] | 51,548/1,689 | 67,947/1,758 | 38,345/1,205 |
| Resolution (Å) | 50–3.15 | 44–2.8 | 50–3.4 |
| $R_{work}/R_{free}$ | 25.3/27.5 | 23.9/25.1 | 24.0/27.3 |
| Rms deviation from ideality | | | |
| Bond lengths (Å) | | 0.009 | |
| Bond angles | | 1.44° | |
| Dihedral angles | | 26.1° | |
| B factors (rmsd of bonded atoms–main/side chain) | | 3.6/5.9 Å$^2$ | |

[a] F1, A1 at Cornell High Energy Synchrotron Source (CHESS); X25 at National Synchrotron Light Source (Brookhaven National Laboratory); ID19 at Advanced Photon Source (Argonne National Laboratory).
[b] Values for the highest resolution shell are given in parentheses.
[c] The first compound was used as the reference in the heavy atom refinement.

$R_{sym} = \frac{\sum_h \sum_i^{n_h} |\hat{I}_h - I_{h,i}|}{\sum_h \sum_i^{n_h} I_{h,i}}$ with $\hat{I}_h = \frac{1}{n_h} \sum_i^{n_h} I_{h,i}$, where I is the integrated intensity of a given reflection and n is the $n^{th}$ symmetry or Friedel equivalent.

$R_{meas} = \frac{\sum_h \sqrt{\frac{n_h}{n_h - 1}} \sum_1^{n_h} |\hat{I}_h - I_{h,i}|}{\sum_h \sum_i^{n_h} I_{h,i}}$, where $n_h$ is the redundancy.

$R_{iso} = \sum |F_{PH} - F_P| / \sum F_P$, where $F_P$ and $F_{PH}$ are the native and derivative structure factor amplitudes.
Phasing power = <rms heavy atom structure factor>/<rms lack of closure>.
Figure of merit = weighted mean of the cosine of the deviation from $\alpha_{best}$.
[d] Against combined reference structure factors from SHARP.
[e] Based on unmerged data.
[f] No rejections based on I/$\sigma$ ratio.
[g] Represents values after refinement in SHARP.
[h] $R_{anom}$: $\langle ||F_{\lambda i}(+)| - |F_{\lambda i}(-)|| \rangle$ / $\langle (|F_{\lambda i}(+)| + |F_{\lambda i}(-)|) \rangle / 2 \rangle$; resolution range: 50–3.3 Å except $\lambda_4$ where the $d_{min}$ = 3.6 Å.

that would be unlikely if Lys-2 would be fixed in the polar core. Fourth, sequence conservation and mutational sensitivity are the hallmarks of functionally important segments of a given structure, and usually such segments are well-ordered components of a crystal structure. As noted earlier, this is the case in our model, where the conserved and mutationally sensitive residues of the C tail make well-defined interactions, which we posit are central to arrestin's regulatory mechanism. The C-terminal tail (369–404) is not visible in the previously reported structure. Finally, it is unlikely that the discrepancies described above arise from differences in crystal forms. We have independently solved and partially refined the same crystal form (P) as that used in the previous report and find that the apparent disorder of the N terminus and structure of the C tail are the same in the P form as in the C form (presented in detail in this report).

### Receptor Binding

Figure 7A illustrates the distribution of electrostatic potential of arrestin. The N domain contains a significant region of positive potential. The positively charged residues in helix I (Arg-102, Lys-109, and Lys-110), which give rise to the tear-shaped potential, are conserved, highly accessible, and undergo no ion pairing. Neither lysine is protected from chemical modification upon arrestin binding to rhodopsin, making it unlikely that they participate in receptor binding (Ohguro et al., 1994b). This lack of interaction suggests that their role might be purely electrostatic, providing the necessary positive potential to orient arrestin with respect to the negatively charged membrane surface. The N domain's proposed proximity to the membrane would facilitate interactions with the phosphorylated tail of rhodopsin by way of a contiguous channel of positive potential that leads to the polar core (Figure 7A).

Arrestin's receptor binding is the ultimate step in the quenching of rhodopsin activity. We propose that a reorientation of the N and C domains presents both of their respective surfaces for association with rhodopsin. The involvement of both domains in the binding is supported by the available evidence as outlined below and is in contrast to the model presented by Granzin and coworkers (1998).

Truncation and deletion studies implicated the N domain as a primary domain of interaction, but that data also showed that the C domain was also likely to play a significant role in the binding (Gurevich and Benovic, 1993). More recent experiments, which involved construction of chimeric molecules of visual arrestin and β-arrestin (Gurevich et al., 1995), furnish a more convincing demonstration that both the N and C domains play a role in binding the activated, phosphorylated receptor. Arrestin was divided approximately into the N terminus, N domain, C domain, and C tail. Both the N and C domains played a dominant role in providing specificity for the cognate receptor, while the N terminus and C tails did not play significant roles in specifying receptor type.

Close analysis of chemical protection experiments of arrestin (Ohguro et al., 1994b) in light of the structure is again consistent with a model where receptor interacts with both domains (Figure 8B). Lysine residues were deuteroacetylated in the presence and absence of light-activated, phosphorylated receptor. Residues on arrestin protected from chemical modification by the receptor mark regions that are most likely to be in contact with rhodopsin. These residues are found on both domains. Moreover, approximately 70 Å separates patches of protected lysine residues in each domain, while the entire cytosolic surface of rhodopsin spans less than 40 Å (Schertler and Hargrave, 1995). This implies that the activated form of arrestin must make a major conformational adjustment to protect lysine side chains in both domains upon binding to receptor. It will be necessary to pursue other approaches such as alanine scanning mutagenesis in order to better define the residues required for receptor binding and specificity. However, taken together these results are consistent with our proposal that after the phosphorylated receptor's C-terminal segment interacts, a cooperative conformational switch occurs which alters the orientation between N and C domains, thereby potentiating binding of both domains to the receptor.

### Conclusions

The biomedical importance of the desensitization machinery in GPCR signaling is only now fully coming to light. Malfunctioning of receptor phosphorylation has been implicated in cardiac pathology (Koch et al., 1995) and hypertension (Gros et al., 1997). More specifically in the visual system, the requirement for receptor phosphorylation to obtain rapid quenching of the photoresponse was shown with mice containing a truncated rhodopsin gene that lacked the C-terminal segment containing the sites of phosphorylation (Chen et al., 1995). Furthermore, mutations in the human arrestin gene are believed to be responsible for a rare autosomal form of stationary night blindness called Oguchi's disease (Fuchs et al., 1995). In parallel with this discovery, transgenic arrestin knockout mice were shown to have prolonged photoresponses, consistent with the human genetic data (Xu et al., 1997).

Based on the structural data presented here in combination with other experiments, we have proposed a hypothesis for arrestin's molecular mechanism. Arrestin's basal state is analogous in some respects to that of a zymogenic proprotease that subsequently undergoes activation. Unlike the zymogen, no covalent bonds are broken, but rather the receptor's phosphorylated C-terminal segment induces a conformational change in arrestin to create a binding-competent form that binds selectively to the cytosolic surface of the activated receptor. The exact nature of arrestin's activated conformation and the stereochemistry of receptor recognition awaits the elucidation of the structure of a receptor–arrestin complex.

### Experimental Procedures

#### Expression and Purification of Arrestin

Recombinant arrestin was expressed and purified as described (C. S. et al., submitted). Selenomethionine-substituted arrestin was expressed in the methionine auxotroph *E. coli* strain B834 (Novagen) in a MOPS-based minimal media (Neidhardt et al., 1974), supplemented with 50 mg $l^{-1}$ L-selenomethionine (Sigma). Purification was carried out as for unsubstituted arrestin except that all buffers were

sparged with argon to prevent oxidation and the protein was immediately used for crystallization. Selenomethionine substitution was confirmed by mass spectrometry.

### Crystallization

Crystals were grown using the hanging drop method and microseeding at 4°C. The reservoir solution consisted of 100 mM Tris-HCl (pH 8.5–8.8), 200 mM ammonium or sodium acetate, and 22%–25% isopropanol. Microseeding stock was prepared by crushing two or three large crystals in a stabilizing supernatant of 100 mM Tris-HCl (pH 8.5–8.8), 200 mM ammonium acetate or sodium acetate, and 30% isopropanol and diluting the suspension serially. Protein stock (1–4 μl at 10 mg $ml^{-1}$) was mixed with reservoir and microseed solution in a ratio of 2:1:1, respectively. Crystals grew within 1 week to an average final size of approximately 50 × 250 × 250 μm. Heavy atom soaks were prepared by adding concentrated heavy atom solutions (listed in Table 1) directly to drops (initial volume = 2–3 μl) containing crystals after addition of 2 μl of reservoir solution. Crystals were frozen by transfer (several seconds) into cryoprotectant solution (100 mM Tris-HCl [pH 8.5], 200 mM ammonium or sodium acetate, 40% isopropanol, 14% xylitol) and then immersion in liquid propane. For the preparation of native and selenomethionyl protein crystals, the cryoprotectant also contained 1–10 mM magnesium acetate, which reduced anisotropic mosaic spread to tolerable values (~1°). "Pseudo native" crystals with improved diffraction quality were obtained by adjusting the drop concentration to 10 mM lead(II) acetate. In the majority of cases, arrestin crystallized in space group $C222_1$ (C form) with typical cell dimensions of a = 168 Å, b = 193 Å, c = 191 Å. The same conditions also yielded a primitive orthorhombic form in space group $P2_12_12$ with cell dimensions a = 168.4 Å, b = 187.8 Å, c = 90.5 Å (P form).

### Data Collection and Structure Determination

The MAD experiment used recombinant selenomethionyl arrestin, while MIRAS experiments used heavy atom derivatized crystals. Due to the weak inherent order of both crystal forms, usable data were obtained only at insertion device synchrotron sources. Therefore, the MAD experiment required an undulator beamline in order to provide sufficient intensity for accurate measurement of the Bijvoet pairs.

Native and derivative data were collected at 100 K with synchrotron radiation as detailed in Table 1. The oscillation range was usually 0.3° to 0.5° except for data from the F1 beamline (CHESS) where 1° oscillations were used. For heavy atom derivatives, the wavelength was tuned where possible to the absorption edge and the inverse beam technique was used to collect the Friedel pairs. A four-wavelength selenomethionine (MAD) experiment (Hendrickson, 1991) was performed on the ID19 beamline at Advanced Photon Source. Data were collected at the anticipated peak of the absorption edge ($\lambda_1$), its presumed inflection point ($\lambda_2$), and low ($\lambda_3$) and high ($\lambda_4$) energy remote points. (Subsequent data analysis indicated that, due to flawed fluorescence spectra, both $\lambda_1$ and $\lambda_2$ data sets straddled the Se absorption peak.) All data sets were processed with DENZO and SCALEPACK (Otwinowski and Minor, 1997).

Crystals of the C form showed a high degree of nonisomorphism between data sets, manifesting itself in a high $R_{merge}$ of up to 40% (based on intensities) and a 2% variation of cell dimensions, especially the b axis. This nonisomorphism made it necessary to divide the data sets into two more isomorphous subclasses and to pursue the structure determination and refinement of these subclasses separately.

In both crystal forms, the asymmetric unit contains four copies of arrestin, resulting in solvent contents of 71% and 69% for the C and P forms, respectively. Self-rotation functions in GLRF (Tong and Rossmann, 1990) and POLARRFN (Collaborative Computational Project Number 4, 1994) revealed in both space groups a major noncrystallographic two-fold rotation axis (64% of the origin peak height) at a 45° angle to the a and c axes.

A subset of selenium positions was identified using the heavy atom search in CNS (Brünger et al., 1998) of averaged anomalous difference Patterson syntheses from $\lambda_1$, $\lambda_2$, and $\lambda_4$. A phase set was computed with PHASES (Furey and Swaminathan, 1997) using the anomalous differences arising from 12 Se sites at three wavelengths. A complete and self-consistent set of sites was developed for the selenium, iridium, and ethyl mercury derivatives by cross-difference Fourier analysis at low resolution. At that stage, derivative (additional derivatives as listed in Table 1 were identified by cross-difference Fourier analysis) and native data sets with an $R_{merge} < 20\%$ were combined into one of two classes and the phase determination branched. One phase set (class A) was obtained from the selenomethionine derivative (MAD), a native, and two other heavy atom derivatives. The other phase set (class B) was derived from the isomorphous differences between the parent and heavy atom derivatives augmented by the associated single wavelength Bijvoet differences of the derivatives (MIRAS). PHASES was used to prepare an initial solvent-flattened map based on isomorphous and Bijvoet differences from class A data. This map clearly showed the noncrystallographic two-fold and polypeptide chain. Final heavy atom and MAD refinement of both classes utilized SHARP (de La Fortelle and Bricogne, 1997). Refinement of class A data was aided by phase information from the nonisomorphous class B phase set, and phases from both classes were improved by density modification (SOLOMON) (Abrahams and Leslie, 1996). Two-fold averaging in RAVE (Kleywegt and Jones, 1994) improved side chain definition in some areas of the maps but did not significantly improve main chain density. The use of selenium positions during model building in O (Jones et al., 1991) and the excellent quality of the electron density maps enabled approximately 90%–95% of the model, including side chains, to be built from both the class A and B experimental maps independently in the first round. Refinement of both models in CNS, guided by the $R_{free}$ (Brünger, 1992) consisted of multiple cycles of torsion angle simulated annealing and B factor refinement including bulk solvent correction and manual rebuilding. The models were restrained tightly to their noncrystallographic two-fold symmetry except for regions that were clearly different due to differing packing environments as judged by σA weighted 2Fo-Fc difference maps. Stereochemical tests by PROCHECK (Laskowski et al., 1993) indicate that the structure is within the idealized targets for its resolution. The two structures produced in the branched phasing scheme are essentially identical with an rmsd of 0.6 Å for corresponding Cα atoms.

The structure of the primitive (P) crystal form was solved by molecular replacement with CNS using a partially refined model of the C form (tetrameric model) as a search structure. A fast direct rotation search showed a top peak (correlation coefficient = 16.6%) 4.3 times greater than the next peak. A translation search gave a solution with a 61% correlation coefficient. Refinement of the four molecules as rigid bodies resulted in an R factor of 36%. Subsequently, the model was refined as above. Composite simulated annealing omit maps were used to confirm that the molecular models were essentially the same in the C and P forms. In particular, there was no density observed for the first amino-terminal eight residues, and the C tail is represented by contiguous density with appreciable side chain density in σA weighted 2Fo-Fc difference maps.

### Acknowledgments

This paper is dedicated to the memory of our colleague and friend, Serge Pares, who helped initiate this project. He and his wife are deeply missed. We are indebted to members of the Sigler lab for their help in data collection (R. Albright, R. Gaudet, T. Kawashima, Y. Korkhin, G. Meinke, and F. Tsai). We thank the staffs of NSLS (Dr. L. Berman and Dr. M. Capel), MacCHESS, and APS-SBC (Dr. A. Joachimiak), Dr. W. Minor and Dr. Z. Otwinowski for a prerelease of HKL2000, Dr. G. Olack for mass spectrometry, Dr. E. de la Fortelle for advice on use of SHARP, and Dr. P. Adams for help with CNS. The work at Yale is supported in part from a grant to P. B. S. (GM22324) from the National Institutes of Health and in Sun City from a National Institutes of Health grant to V. V. G. (EY11500). J. A. H. is a National Eye Institute postdoctoral fellow, and C. S. is a Fellow of the Deutsche Forschungsgemeinschaft.

Received February 1, 1999; revised March 15, 1999.

### References

Abrahams, J.P., and Leslie, A.G.W. (1996). Methods used in the structure determination of bovine mitochondrial F-1 ATPase. Acta Crystallogr. *D52*, 30–42.

Aton, B.R., Litman, B.J., and Jackson, M.L. (1984). Isolation and identification of the phosphorylated species of rhodopsin. Biochemistry *23*, 1737–1741.

Azarian, S.M., King, A.J., Hallett, M.A., and Williams, D.S. (1995). Selective proteolysis of arrestin by calpain. Molecular characteristics and its effect on rhodopsin dephosphorylation. J. Biol. Chem. *270*, 24375–24384.

Brünger, A.T. (1992). Free R-value: a novel statistical quantity for assessing the accuracy of crystal structures. Nature *355*, 472–475.

Brünger, A.T., Adams, P.D., Clore, G.M., DeLano, W.L., Gros, P., Grosse-Kunstleve, R.W., Jiang, J.S., Kuszewski, J., Nilges, M., Pannu, N.S., et al. (1998). Crystallography and NMR system: a new software suite for macromolecular structure determination. Acta Crystallogr. *D54*, 905–921.

Carrell, R.W., Stein, P.E., Fermi, G., and Wardell, M.R. (1994). Biological implications of a 3 Å structure of dimeric antithrombin. Structure *2*, 257–270.

Chen, J., Makino, C.L., Peachey, N.S., Baylor, D.A., and Simon, M.I. (1995). Mechanisms of rhodopsin inactivation in vivo as revealed by a COOH-terminal truncation mutant. Science *267*, 374–377.

Collaborative Computational Project Number 4. (1994). The CCP4 suite: programs for protein crystallography. Acta Crystallogr. *D50*, 760–763.

de La Fortelle, E., and Bricogne, G. (1997). Maximum-likelihood heavy atom parameter refinement for multiple isomorphous replacement and multiwavelength anomalous diffraction methods. Methods Enzymol. *276*, 472–494.

Fuchs, S., Nakazawa, M., Maw, M., Tamai, M., Oguchi, Y., and Gal, A. (1995). A homozygous 1-base pair deletion in the arrestin gene is a frequent cause of Oguchi disease in Japanese. Nat. Genet. *10*, 360–362.

Furey, W., and Swaminathan, S. (1997). PHASES-95: a program package for processing and analyzing diffraction data from macromolecules. Methods Enzymol. *277*, 590–620.

Gerstein, M., and Levitt, M. (1998). Comprehensive assessment of automatic structural alignment against a manual standard, the SCOP classification of proteins. Prot. Sci. *7*, 445–456.

Granzin, J., Wilden, U., Choe, H.W., Labahn, J., Krafft, B., and Buldt, G. (1998). X-ray crystal structure of arrestin from bovine rod outer segments. Nature *391*, 918–921.

Gros, R., Benovic, J.L., Tan, C.M., and Feldman, R.D. (1997). G protein-coupled receptor kinase activity is increased in hypertension. J. Clin. Invest. *99*, 2087–2093.

Gurevich, V.V. (1998). The selectivity of visual arrestin for light-activated phosphorhodopsin is controlled by multiple nonredundant mechanisms. J. Biol. Chem. *273*, 15501–15506.

Gurevich, V.V., and Benovic, J.L. (1993). Visual arrestin interaction with rhodopsin. Sequential multisite binding ensures strict selectivity toward light-activated phosphorylated rhodopsin. J. Biol. Chem. *268*, 11628–11638.

Gurevich, V.V., and Benovic, J.L. (1997). Mechanism of phosphorylation-recognition by visual arrestin and the transition of arrestin into a high affinity binding state. Mol. Pharmacol. *51*, 161–169.

Gurevich, V.V., Chen, C.Y., Kim, C.M., and Benovic, J.L. (1994). Visual arrestin binding to rhodopsin. Intramolecular interaction between the basic N terminus and acidic C terminus of arrestin may regulate binding selectivity. J. Biol. Chem. *269*, 8721–8727.

Gurevich, V.V., Dion, S.B., Onorato, J.J., Ptasienski, J., Kim, C.M., Sterne-Marr, R., Hosey, M.M., and Benovic, J.L. (1995). Arrestin interactions with G protein-coupled receptors. Direct binding studies of wild type and mutant arrestins with rhodopsin, beta 2-adrenergic, and m2 muscarinic cholinergic receptors. J. Biol. Chem. *270*, 720–731.

Hamm, H.E., and Bownds, M.D. (1986). Protein complement of rod outer segments of frog retina. Biochemistry *25*, 4512–4523.

Hendrickson, W.A. (1991). Determination of macromolecular structures from anomalous diffraction of synchrotron radiation. Science *254*, 51–58.

Hendsch, Z.S., and Tidor, B. (1994). Do salt bridges stabilize proteins? A continuum electrostatic analysis. Prot. Sci. *3*, 211–226.

Holm, L., and Sander, C. (1998). Touring protein fold space with Dali/FSSP. Nucleic Acids Res. *26*, 316–319.

Jones, S., and Thornton, J.M. (1995). Protein-protein interactions: a review of protein dimer structures. Prog. Biophys. Mol. Biol. *63*, 31–65.

Jones, T.A., Zou, J.-Y., Cowan, S.W., and Kjeldgaard, M. (1991). Improved methods for building protein models in electron density maps and the location of errors in these models. Acta Crystallogr. *A47*, 110–119.

Kabsch, W., and Sander, C. (1983). Dictionary of protein secondary structure: pattern recognition of hydrogen-bonded and geometrical features. Biopolymers *22*, 2577–2637.

Kawamura, S. (1995). Phototransduction, excitation and adaption. In Neurobiology and Clinical Aspects of the Outer Retina, M.B.A. Djamangoz, S.N. Archer, and S. Vallerga, eds. (London: Chapman and Hall), pp. 105–131.

Kleywegt, G.J., and Jones, T.A. (1994). Halloween ... masks and bones. In From First Map to Final Model, S. Bailey, R. Hubbard, and D. Waller, eds. (Warrington: SERC Daresbury Laboratory), pp. 59–66.

Koch, W.J., Rockman, H.A., Samama, P., Hamilton, R.A., Bond, R.A., Milano, C.A., and Lefkowitz, R.J. (1995). Cardiac function in mice overexpressing the beta-adrenergic receptor kinase or a beta ARK inhibitor. Science *268*, 1350–1353.

Kraulis, P. (1991). MOLSCRIPT: a program to produce both detailed and schematic plots of protein structures. J. Appl. Crystallogr. *24*, 946–950.

Krupnick, J.G., and Benovic, J.L. (1998). The role of receptor kinases and arrestins in G protein-coupled receptor regulation. Annu. Rev. Pharmacol. Toxicol. *38*, 289–319.

Krupnick, J.G., Goodman, O.B., Jr., Keen, J.H., and Benovic, J.L. (1997). Arrestin/clathrin interaction. Localization of the clathrin binding domain of nonvisual arrestins to the carboxy terminus. J. Biol. Chem. *272*, 15011–15016.

Laskowski, R.A., MacArthur, M.W., Moss, D.S., and Thorton, J.M. (1993). PROCHECK: a program to check the stereochemical quality of protein structures. J. Appl. Crystallogr. *26*, 283–291.

Lee, B., and Richards, F.M. (1971). The interpretation of protein structures: estimation of static accessibility. J. Mol. Biol. *55*, 379–400.

Lefkowitz, R.J. (1998). G protein-coupled receptors: III. new roles for receptor kinases and β-arrestins in receptor signaling and desensitization. J. Biol. Chem. *273*, 18677–18680.

Lim, W.A., and Sauer, R.T. (1989). Alternative packing arrangements in the hydrophobic core of lambda repressor. Nature *339*, 31–36.

Matthews, B.W. (1995). Studies on protein stability with T4 lysozyme. Adv. Prot. Chem. *46*, 249–278.

McDowell, J.H., Nawrocki, J.P., and Hargrave, P.A. (1993). Phosphorylation sites in bovine rhodopsin. Biochemistry *32*, 4968–4974.

Merritt, E.A., and Bacon, D.J. (1997). Raster3D: photorealistic molecular graphics. Methods Enzymol. *277*, 505–524.

Minor, D.L., Jr., and Kim, P.S. (1996). Context-dependent secondary structure formation of a designed protein sequence. Nature *380*, 730–734.

Myers, E.W., and Miller, W. (1988). Optimal alignments in linear space. Comput. Appl. Biosci. *4*, 11–17.

Neidhardt, F.C., Bloch, P.L., and Smith, D.F. (1974). Culture medium for enterobacteria. J. Bacteriol. *119*, 736–747.

Nicholls, A., Sharp, K., and Honig, B. (1991). Protein folding and association: insights from the interfacial and thermodynamic properties of hydrocarbons. Proteins *11*, 281–296.

Ohguro, H., Johnson, R.S., Ericsson, L.H., Walsh, K.A., and Palczewski, K. (1994a). Control of rhodopsin multiple phosphorylation. Biochemistry *33*, 1023–1028.

Ohguro, H., Palczewski, K., Walsh, K.A., and Johnson, R.S. (1994b). Topographic study of arrestin using differential chemical modifications and hydrogen/deuterium exchange. Prot. Sci. *3*, 2428–2434.

Ohguro, H., Van Hooser, J.P., Milam, A.H., and Palczewski, K. (1995). Rhodopsin phosphorylation and dephosphorylation in vivo. J. Biol. Chem. *270*, 14259–14262.

Otwinowski, Z., and Minor, W. (1997). Processing of X-ray diffraction data collected in oscillation mode. Methods Enzymol. *276*, 307–325.

Palczewski, K., Pulvermüller, A., Buczylko, J., and Hofmann, K.P. (1991a). Phosphorylated rhodopsin and heparin induce similar conformational changes in arrestin. J. Biol. Chem. *266*, 18649–18654.

Palczewski, K., Buczylko, J., Imami, N.R., McDowell, J.H., and Hargrave, P.A. (1991b). Role of the carboxyl-terminal region of arrestin in binding to phosphorylated rhodopsin. J. Biol. Chem. *266*, 15334–15339.

Palczewski, K., Buczylko, J., Ohguro, H., Annan, R.S., Carr, S.A., Crabb, J.W., Kaplan, M.W., Johnson, R.S., and Walsh, K.A. (1994). Characterization of a truncated form of arrestin isolated from bovine rod outer segments. Prot. Sci. *3*, 314–324.

Puig, J., Arendt, A., Tomson, F.L., Abdulaeva, G., Miller, R., Hargrave, P.A., and McDowell, J.H. (1995). Synthetic phosphopeptide from rhodopsin sequence induces retinal arrestin binding to photoactivated unphosphorylated rhodopsin. FEBS Lett. *362*, 185–188.

Pulvermüller, A., Maretzki, D., Rudnicka-Nawrot, M., Smith, W.C., Palczewski, K., and Hofmann, K.P. (1997). Functional differences in the interaction of arrestin and its splice variant, $p^{44}$, with rhodopsin. Biochemistry *36*, 9253–9260.

Schertler, G.F., and Hargrave, P.A. (1995). Projection structure of frog rhodopsin in two crystal forms. Proc. Natl. Acad. Sci. USA *92*, 11578–11582.

Schleicher, A., Kühn, H., and Hofmann, K.P. (1989). Kinetics, binding constant, and activation energy of the 48-kDa protein-rhodopsin complex by extra-metarhodopsin II. Biochemistry *28*, 1770–1775.

Schreuder, H.A., de Boer, B., Dijkema, R., Mulders, J., Theunissen, H.J., Grootenhuis, P.D., and Hol, W.G. (1994). The intact and cleaved human antithrombin III complex as a model for serpin-proteinase interactions. Nat. Struct. Biol. *1*, 48–54.

Sindelar, C.V., Hendsch, Z.S., and Tidor, B. (1998). Effects of salt bridges on protein structure and design. Prot. Sci. *7*, 1898–1914.

Tan, S., and Richmond, T.J. (1998). Crystal structure of the yeast MATalpha2/MCM1/DNA ternary complex. Nature *391*, 660–666.

Tong, L., and Rossmann, M. (1990). The locked rotation function. Acta Crystallogr. *A46*, 783–792.

Vishnivetskiy, S.A., Paz, C.L., Schubert, C., Hirsch, J.A., Sigler, P.B., and Gurevich, V.V. (1999). How does arrestin respond to the phosphorylated state of rhodopsin? J. Biol. Chem. *274*, 11451–11454.

Waldburger, C.D., Schildbach, J.F., and Sauer, R.T. (1995). Are buried salt bridges important for protein stability and conformational specificity? Nat. Struct. Biol. *2*, 122–128.

Wimley, W.C., Gawrisch, K., Creamer, T.P., and White, S.H. (1996). Direct measurement of salt-bridge solvation energies using a peptide model system: implications for protein stability. Proc. Natl. Acad. Sci. USA *93*, 2985–2990.

Xu, J., Dodd, R.L., Makino, C.L., Simon, M.I., Baylor, D.A., and Chen, J. (1997). Prolonged photoresponses in transgenic mouse rods lacking arrestin. Nature *389*, 505–509.

**Protein Data Bank ID Code**

Coordinates have been deposited with the ID code 1cf1.

**Note Added in Proof**

The data referred to throughout as ''C.S. et al., submitted'' are now in press: Schubert, C., Hirsch, J.A., Gurevich, V.V., Engelman, D.M., and Sigler, P.B. (1999). Visual arrestin activity may be regulated by self-association. J. Biol. Chem.